Bifurcations in a modulation equation for alternans in a cardiac fiber

Shu Dai and David G. Schaeffer
Department of Mathematics and Center for Nonlinear and Complex Systems,
Duke University, Durham, NC 27708 USA

September 29, 2008

Abstract

While alternans in a single cardiac cell appears through a simple period-doubling bifurcation, in extended tissue the exact nature of the bifurcation is unclear. In particular, the phase of alternans can exhibit wave-like spatial dependence, either stationary or traveling, which is known as *discordant* alternans. We study these phenomena in simple cardiac models through a modulation equation proposed by Echebarria-Karma. As shown in our previous paper, the zero solution of their equation may lose stability, as the pacing rate is increased, through either a Hopf or steady-state bifurcation. Which bifurcation occurs first depends on parameters in the equation, and for one critical case both modes bifurcate together at a degenerate (codimension 2) bifurcation. For parameters close to the degenerate case, we investigate the competition between modes, both numerically and analytically. We find that at sufficiently rapid pacing (but assuming a 1:1 response is maintained), steady patterns always emerge as the only stable solution. However, in the parameter range where Hopf bifurcation occurs first, the evolution from periodic solution (just after the bifurcation) to the eventual standing wave solution occurs through an interesting series of secondary bifurcations.

1 Introduction

An abnormal cardiac rhythm known as *alternans*, a bifurcation of the action potential duration (APD) of cardiac cells under rapid pacing stimuli, is believed to be one precursor of life-threatening ventricular fibrillation and sudden cardiac death[1, 2, 3]. The APD in a single paced cell has been modelled by the following restitution relationship [4, 5]:

$$A_{n+1} = f(DI_n), \tag{1.1}$$

i.e. the APD only depends on the previous diastolic interval (DI), where A_n denotes the n^{th} APD. In such a model alternans appears as a period-doubling bifurcation.

In extended tissue composed of multiple cardiac cells, the action potentials generated by the stimuli will propagate in the tissue. Since the conduction velocity (CV) depends on the DI, the APD of the cell will also be a function of the cell's position. In the case of one dimension, suppose we have a cardiac fiber of length L, which is stimulated periodically at its $x = 0$ end, say with period B. Assume each stimulus successfully generates an action potential that propagates down the fiber. Let $A_n(x)$ be the duration of the n^{th} action potential at the position x along the fiber. If the pacing is rapid such that the basic cycle length B is below the critical value B_{crit}, alternans are expected. To analyze position-dependent APD's, Echebarria and Karma made the ansatz [6]:

$$A_n(x) = A_{\text{crit}} - \delta A + (-1)^n a_n(x), \tag{1.2}$$

where A_{crit} is the APD when pacing with period $B = B_{\text{crit}}$, δA is the average shortening of APD resulting from decreasing B below B_{crit} and $a_n(x)$ is the amplitude of n^{th} alternans. It is assumed that $a_n(x)$ varies slowly from beat to beat thus one may regard it as the discrete values of a smooth function $a(x,t)$ of smooth time t, i.e. $a_n(x) = a(x, t_n)$ where $t_n = n \cdot B$ for $n = 0, 1, 2 \ldots$ when stimuli are applied. A weakly nonlinear modulation equation for $a(x,t)$ was derived in [6], which after the nondimensionization with respect to time, is given by

$$\partial_t a = \sigma a + \xi^2 \partial_{xx} a - w \partial_x a - \frac{1}{\Lambda} \int_0^x a(x', t) dx' - g a^3, \tag{1.3}$$

where σ is the bifurcation parameter, which is dimensionless and proportional to $B_{\text{crit}} - B$; Λ, w, ξ are positive parameters, each having the units of length, that are derived from the equations of the cardiac model; and the nonlinear term $-ga^3$ limits growth after the onset of linear instability. Neumann boundary conditions

$$\partial_x a(0, t) = 0, \quad \partial_x a(l, t) = 0 \tag{1.4}$$

are imposed on (1.3).

The trivial steady state solution $a \equiv 0$ of (1.3-1.4) loses its stability as σ increases. In the previous paper [8], we analyzed the eigenvalues of the linear operator that maps a function $a(x)$ to

$$\xi^2 a'' - w a' - \frac{1}{\Lambda} \int_0^x a(x') dx', \tag{1.5}$$

subject to Neumann boundary conditions, and we concluded that the first bifurcation we observe as σ increases may be steady state bifurcation if $\Lambda^{-1} < \Lambda_c^{-1}$ or Hopf bifurcation otherwise, where the critical value Λ_c^{-1} depends on L, w and ξ. In this paper, extending our previous result, we simulate and analyze the bifurcation of (1.3) when Λ^{-1} is close to Λ_c^{-1} and hence competition of multiple modes appear.

The organization of this paper is the following: Section 2 reviews our previous result on the bifurcation from a simple eigenvalue. Section 3 shows the simulated results for the dynamics of the solution for Λ^{-1} around Λ_c^{-1}. In Sections 4-5 we show that the dynamics of (1.3) may be derived from a reduced three dimensional flow. In Section 6 we perform a bifurcation analysis and relate it to the simulations.

Incidentally, in a future paper we will show that for Λ^{-1} in a broader neighborhood of Λ_c^{-1}, more complicated dynamics is obtained, possibly including chaos.

2 Linear Stability: Bifurcation from a Simple Eigenvalue

We follow the nondimensionization steps as in [8]: if we define dimensionless variables

$$\bar{w} = w \cdot \xi^{-1}, \quad \bar{\Lambda} = \Lambda \cdot w^3 \xi^{-4}, \quad \bar{x} = x \cdot w\, \xi^{-2}, \quad \bar{l} = l \cdot w\, \xi^{-2}, \tag{2.1}$$

then the operator in (1.5) can be written as $w^2 \xi^{-2} \cdot \mathbf{L}a$, where

$$\mathbf{L}a = \frac{d^2 a}{d\bar{x}^2} - \frac{da}{d\bar{x}} - \bar{\Lambda}^{-1} \int_0^{\bar{x}} a(\bar{x}') d\bar{x}'. \tag{2.2}$$

For convenience below we will omit all the bars in (2.2). The boundary conditions are

$$a'(0) = 0, \quad a'(l) = 0. \tag{2.3}$$

where l is the dimensionless length of the cardiac fiber.

Obviously $a(x,t) \equiv 0$ is a trivial solution to (1.3). When σ is small (including all negative values), the zero solution is linearly stable. As σ increases to beyond some threshold, the zero solution loses its stability. To investigate the bifurcation, we consider the eigenvalues of the linear operator (2.2). Suppose $\Omega_0, \Omega_1, \Omega_2, \ldots$ are those eigenvalues and let $\Omega_{\max}$ be the one having the largest real part. If $\sigma + \operatorname{Re}\Omega_{\max} < 0$, the zero solution is linearly stable; otherwise it is unstable. This bifurcation at $\sigma = -\operatorname{Re}\Omega_{\max}$ can be either steady state or Hopf, depending on whether $\Omega_{\max}$ is real or complex.

The dimensionless linear operator (2.2), together with the boundary conditions (2.3) has two parameters l and Λ. In our previous paper [8], we found that for l sufficiently large, as Λ^{-1} varies, the eigenvalues of (2.2) behave as illustrated in Figure 1. In the figure $l = 6$ and only the real parts of all eigenvalues are graphed (Remark: In [8] we computed the eigenvalues asymptotically for large l). By the critical value of Λ^{-1}, say Λ_c^{-1}, as denoted in the graph, we mean the crossover point where the eigenvalue with largest real part $\Omega_{\max}$ changes from real to complex.

We observe that all eigenvalues lie in the left half of the complex plane, i.e. they all have negative real parts. When $\Lambda^{-1} < \Lambda_c^{-1}$, $\Omega_{\max} = \Omega_0$. Since Ω_0 is real, as σ increases from 0, we will first encounter a steady state bifurcation at $\sigma = |\operatorname{Re}\Omega_{\max}| = -\Omega_0$, and as we compute below

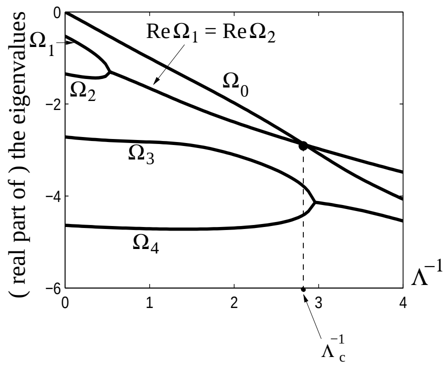

Figure 1: The evolution of the real parts of the first five eigenvalues $\Omega_0, \Omega_1 \ldots \Omega_4$ of the linear operator in (2.2) vs. Λ^{-1}, assuming $l = 6$. All eigenvalues are real for Λ^{-1} sufficiently small, but, except for Ω_0, they become complex as Λ^{-1} increases. $\Lambda_c^{-1} \approx 2.837$ is the crossover point such that if $\Lambda^{-1} > \Lambda_c^{-1}$ the eigenvalue which has largest real part, $\Omega_{\max}$, is complex.

beyond the bifurcation point the solution to equation (1.3) has a stable pattern of standing waves. On the other hand if $\Lambda^{-1} > \Lambda_c^{-1}$, we have $\Omega_{\max} = \Omega_{1,2}$, which is a complex pair and as σ increases from 0 we will encounter a Hopf bifurcation at $\sigma = |\mathrm{Re}\,\Omega_{\max}| = -\mathrm{Re}\,\Omega_1$, and at least for a small range of σ beyond the bifurcation point the solution has a propagating pattern. A calculation in [8] shows that for sufficiently large L, to the leading order, the dimensionless critical value equals

$$\Lambda_c^{-1} = \frac{71 + 17\sqrt{17}}{64} + \mathcal{O}(l^{-2}). \tag{2.4}$$

In the critical case, i.e. when $\Lambda^{-1} = \Lambda_c^{-1}$, we have $\Omega_0 = \mathrm{Re}\,\Omega_{1,2}$, both modes become unstable simultaneously. In the next section we investigate numerically the behavior of the system near such a degenerate point.

3 Competition between Modes Near the Critical Point

In the following sections we fix the dimensionless length of the cardiac fiber to be $l = 6$ to illustrate the dynamics. We find by computation that for $l = 6$, the critical point $\Lambda_c^{-1} \approx 2.837$.

Figure 2A illustrates the simulation results of the dynamics of the solution to the modulation equation (1.3) when Λ^{-1} is near the critical value Λ_c^{-1}. If (Λ^{-1}, σ) lies in the quasitriangular region (3) in Figure 2A, the stable solution of (1.3) is a steady pattern; for example the solution corresponding to point Y in Figure 2A is illustrated in Figure 2B (upper). If $\Lambda^{-1} < \Lambda_c^{-1}$ is fixed and σ crosses into region (3), this steady solution appears through a single, simple bifurcation as

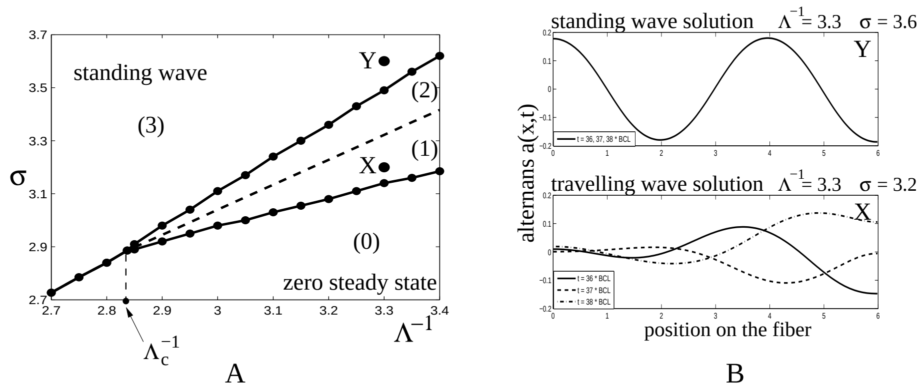

Figure 2: **A**: The bifurcation diagram for Λ^{-1} near Λ_c^{-1} when $l = 6$. There are four regions each denoting different behavior of the solution: (0), trivial zero steady state solution, (1), pure periodic solution, (2), mixed-mode periodic solution and (3) standing wave solution. **B**: Two simulated solutions whose parameters correspond to X and Y in Figure 2A. The upper one is a standing wave and the lower one has a travelling pattern

discussed in Section 2. However if $\Lambda^{-1} > \Lambda_c^{-1}$ is fixed and σ is increased, the situation is more complicated. The first bifurcation is to a periodic solution; for example, the solution corresponding to point X in Figure 2A is illustrated in Figure 2B (lower). However, as σ is increased further, the solution evolves to a steady pattern through two secondary bifurcations.

To better understand this behavior, consider the solution as a function of time at a fixed point x_1. For $x_1 = \frac{15}{20} \times l = 4.5$ and $\Lambda^{-1} = 3.3$ (note that $\Lambda^{-1} > \Lambda_c^{-1}$), Figure 3 shows how the quantity

$$\max_t a(x_1, t) - \min_t a(x_1, t) \tag{3.1}$$

(dashed line) and the average

$$\frac{1}{T} \int_0^T a(x_1, t)\, dt, \tag{3.2}$$

where T is the period (solid line), vary with σ for $3 < \sigma < 3.7$. In region (1), which we call the pure-periodic region, the average of the solution is close to zero. By contrast, in region (2), although the solution continues to oscillate, its average is nonzero. Finally, in region (3) the solution is steady (and equal to its average).

In the following sections we provide supporting theory for the above observation. In particular we shall see that the transitions between region (1) and (2) and between (2) and (3) represent secondary bifurcations that appear from unfolding the degenerate bifurcation for $\Lambda^{-1} = \Lambda_c^{-1}$.

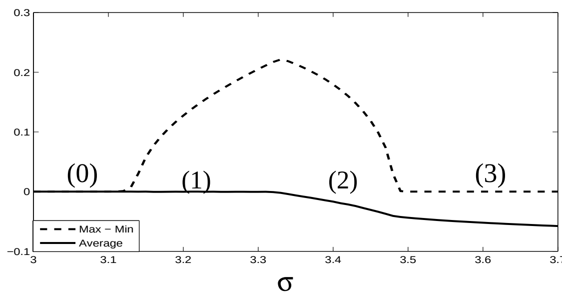

Figure 3: The simulation result for the oscillation amplitude, $\max_t a(x_1,t) - \min_t a(x_1,t)$ (dashed curve), and the average of $a(x_1,t)$ (solid curve) in one period for various values of σ when $\Lambda^{-1} = 3.3$ and $x_1 = \frac{15}{20} \times l = 4.5$. The four labels refer to regions in Figure 2A: (0) for $\sigma < 3.14$, zero steady state solution, both amplitude and average are zero, (1) for $3.14 < \sigma < 3.32$, pure periodic solution, the amplitude is nonzero but the average is zero (to leading order), (2) for $3.32 < \sigma < 3.49$, mixed mode solution, both amplitude and average are nonzero, (3) for $\sigma > 3.49$, standing wave, with no oscillation and nonzero average.

4 Reduction to a Three Dimensional System

We consider the case when the parameter Λ^{-1} exactly equals to the critical value Λ_c^{-1}, so we have

$$\Omega_0 = \operatorname{Re}\Omega_{1,2} > \operatorname{Re}\Omega_{3,4} > \dots,$$

which are all negative. For appropriate σ, we apply center-manifold theory [9, 10] to show that the dynamics of the solution to (1.3) is determined by the first three modes corresponding to $\Omega_{0,1,2}$.

First we rewrite the modulation equation (1.3) in a more convenient way. Define $\tilde{\sigma} = \sigma - \sigma_c$, the increment of σ away from its bifurcation value $\sigma_c = -\Omega_0$. In dimensionless variables, (1.3) can be rewritten as

$$\partial_t a = \tilde{\sigma} a + \mathscr{L} a - a^3, \tag{4.1}$$

where

$$\mathscr{L} a = \sigma_c a + a'' - a' - \Lambda_c^{-1} \int_0^x a(x')dx' \tag{4.2}$$

and we have assumed the positive nonlinear coefficient $g = 1$ by a scaling $a \to g^{-1/2} \cdot a$.

The eigenvalues of $\mathscr{L}$ are $\widetilde{\Omega}_n = \Omega_n + \sigma_c = \Omega_n - \Omega_0$ for $n = 0, 1, 2, \dots$. Thus the first three eigenvalues are all on the imaginary axis:

$$\widetilde{\Omega}_0 = 0,\ \widetilde{\Omega}_{1,2} = \pm \mathbf{i}\,\omega, \tag{4.3}$$

where $\omega > 0$ is real. All other eigenvalues are in the left half plane. Let $\phi_0(x)$ be the eigenfunction with eigenvalue $\widetilde{\Omega}_0$ and $\phi_1(x) \pm \mathbf{i}\,\phi_2(x)$ be the eigenfunctions with eigenvlaues $\widetilde{\Omega}_{1,2}$, i.e.

$$\mathscr{L}\phi_0 = 0 \quad \text{and} \quad \mathscr{L}(\phi_1 \pm \mathbf{i}\,\phi_2) = \pm\mathbf{i}\,\omega(\phi_1 \pm \mathbf{i}\,\phi_2), \tag{4.4}$$

where ϕ_0, ϕ_1, ϕ_2 are all real. Let $E^c = \text{span}\{\phi_0, \phi_1, \phi_2\}$, i.e. E^c is the central subspace. We study the dynamics of $a(x,t)$ through its projection onto the central subspace.

We regard the solution to (4.1) as a flow in the function space of L^2 on the interval $(0, l)$, i.e. square integrable functions. By the central manifold theorem [9, 10], there exists a central manifold $\mathcal{M}$ which is invariant under the flow and tangent to the central space E^c, and there is also a neighborhood of zero in L^2, denoted by U, with the following property: if $a(\cdot, t)$ is a solution of (4.1) such that for all $t > 0$, $a(\cdot, t) \in U$, then the distance from $a(\cdot, t)$ to $\mathcal{M}$ converges to zero exponentially. In other words, to understand the long-time dynamics of (4.1) near 0, it is sufficient to examine the flow on $\mathcal{M}$. The flow on $\mathcal{M}$ is a three dimensional ODE, which can be formulated by using the coordinates of E^c .

We first introduce the adjoint operator of $\mathscr{L}$, which is defined as below:

$$\mathscr{L}^* a = \sigma_c a + a'' + a' - \Lambda_c^{-1} \int_x^l a(x')dx', \tag{4.5}$$

with boundary conditions

$$a'(0) + a(0) = a'(l) + a(l) = 0. \tag{4.6}$$

The adjoint operator $\mathscr{L}^*$ has the same eigenvalues as $\mathscr{L}$. Let ψ_0, $\psi_1 \pm \mathbf{i}\,\psi_2$ be the first three eigenfunctions of $\mathscr{L}^*$, i.e.,

$$\mathscr{L}^*\psi_0 = 0 \quad \text{and} \quad \mathscr{L}^*(\psi_1 \pm \mathbf{i}\,\psi_2) = \mp\mathbf{i}\,\omega \cdot (\psi_1 \pm \mathbf{i}\,\psi_2), \tag{4.7}$$

where ψ_0, ψ_1 and ψ_2 are all real.We may impose the following conditions of orthogonality:

$$\langle \psi_i, \phi_j \rangle = \delta_{ij}, \quad \text{for } \; i, j = 0, 1, 2, \tag{4.8}$$

where the inner product $\langle, \rangle$ is taken in the L^2–sense. Figure 4 shows a possible choice of $\phi_i(x)$ and $\psi_i(x)$ for $i = 0, 1, 2$.

We now parameterize $\mathcal{M}$ by E^c. Let $\mathcal{H} = \{\psi_0, \psi_1, \psi_2\}^\perp$; then $\mathcal{H}$ is a complement of E^c in L^2, i.e. $L^2 \cong E^c \oplus \mathcal{H}$. Let π be the projection onto E^c with kernel $\mathcal{H}$. Since $\mathcal{M}$ is tangent to E^c, for all $u = \sum_{i=0}^{2} u_i \phi_i$ in $E^c \cap U$, there is a unique $J(u) \in \mathcal{M}$ such that $\pi J(u) = u$. Moreover, the difference $R(u) = J(u) - u$ belongs to $\mathcal{H}$ and satisfies

$$R(u) = \mathcal{O}(|u|^2). \tag{4.9}$$

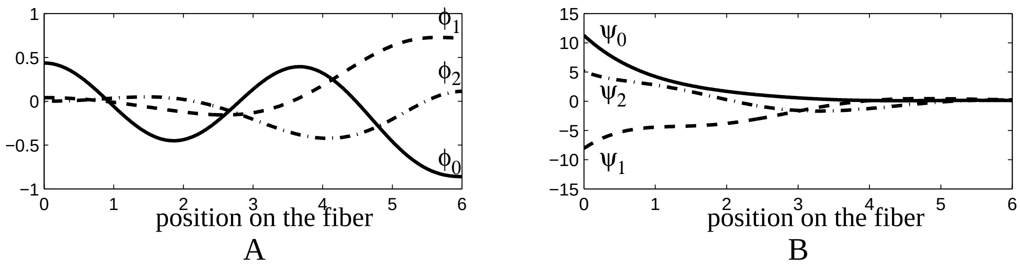

Figure 4: Illustration of the eigenfunctions $\phi_{0,1,2}$ in (4.4) and $\psi_{0,1,2}$ in (4.7) , assuming the length of the fiber $l = 6$. They satisfy the conditions of orthogonality (4.8).

Suppose $a(x, t)$ is a solution of (4.1) such that for all time $a(\cdot, t) \in \mathcal{M} \cap U$. Let $u(t) = \pi a(\cdot, t)$. Of course $a(\cdot, t) = J(u(t))$. To derive an ODE for $u(t)$, we calculate

$$\begin{aligned} \dot{u} = \pi\dot{a} &= \tilde{\sigma}u + \pi\mathscr{L}J(u) - \pi[J(u)^3] \\ &= \tilde{\sigma}u + \pi\mathscr{L}u + \pi\mathscr{L}R(u) - \pi(u^3 + \mathcal{O}(|u|^4)). \end{aligned} \tag{4.10}$$

Clearly $\pi\mathscr{L}u = \mathscr{L}u$ for $\mathscr{L}u \in E^c$ since $u \in E^c$. Since $R(u) \in \mathcal{H}$, for $j = 0, 1, 2$, we have $\langle\psi_j, \mathscr{L}R(u)\rangle = \langle\mathscr{L}^*\psi_j, R(u)\rangle = 0$, i.e. $\mathscr{L}R(u) \in \mathcal{H}$ and hence $\pi\mathscr{L}R(u) = 0$. Thus (4.10) can be rewritten as

$$\dot{u} = \tilde{\sigma}u + \mathscr{L}u - \pi(u^3) + \mathcal{O}(|u|^4). \tag{4.11}$$

Let us regard E^c, a subspace of L^2, as a three-dimensional vector space with coordinates (u_0, u_1, u_2) defined by

$$u = \sum_{i=0}^{2} u_i(t)\phi_i(x).$$

To expand (4.11) in coordinates, we take the inner product of this equation with each ψ_j for $j = 0, 1, 2$. Since $u^3 - \pi(u^3) \in \mathcal{H} = \{\psi_0, \psi_1, \psi_2\}^\perp$, we conclude that $\langle\psi_j, \pi(u^3)\rangle = \langle\psi_j, u^3\rangle$ for $j = 0, 1, 2$. By (4.4) and (4.8), we obtain the ODE system for each coordinate $u_i(t)$:

$$\begin{cases} \dot{u}_0 = \tilde{\sigma}u_0 - \langle\psi_0, (\sum\limits_{i=0}^{2} u_i\phi_i)^3\rangle + \mathcal{O}(|u|^4), \\ \dot{u}_1 = \tilde{\sigma}u_1 - \omega u_2 - \langle\psi_1, (\sum\limits_{i=0}^{2} u_i\phi_i)^3\rangle + \mathcal{O}(|u|^4), \\ \dot{u}_2 = \tilde{\sigma}u_2 + \omega u_1 - \langle\psi_2, (\sum\limits_{i=0}^{2} u_i\phi_i)^3\rangle + \mathcal{O}(|u|^4). \end{cases} \tag{4.12}$$

We expand $(\sum\limits_{i=0}^{2} u_i\phi_i)^3$ in each equation in (4.12), and the coefficient for each term $u_0^{i_0}u_1^{i_1}u_2^{i_2}$, where

(i_0,i_1,i_2)	$3,0,0$	$2,1,0$	$2,0,1$	$1,2,0$	$1,1,1$	$1,0,2$	$0,3,0$	$0,2,1$	$0,1,2$	$0,0,3$
$h^0_{i_0 i_1 i_2}$	0.168	-0.070	-0.346	0.081	0.010	0.582	0.004	-0.053	-0.021	-0.084
$h^1_{i_0 i_1 i_2}$	0.008	0.132	-0.152	-0.104	0.021	0.160	0.107	-0.228	0.262	-0.040
$h^2_{i_0 i_1 i_2}$	0.055	-0.024	-0.188	0.012	0.017	0.146	-0.015	0.023	0.012	0.096

Table 1: Values of the coefficients $h^j_{i_0 i_1 i_2}$ in system (4.14).

$i_0 + i_1 + i_2 = 3$, in the j-th equation is given by

$$h^j_{i_0 i_1 i_2} = \langle \psi_j, \phi_0^{i_0} \phi_1^{i_2} \phi_0^{i_3} \rangle = \int_0^l \psi_j \phi_0^{i_0} \phi_1^{i_2} \phi_0^{i_3}\, dx. \tag{4.13}$$

For instance, $h^1_{2,1,0} = \langle \psi_1, \phi_0^2 \phi_1 \rangle = \int_0^l \psi_1 \phi_0^2 \phi_1\, dx$. Choosing the functions ϕ_i's and ψ_j's as in Figure 4, we computed all the coefficients numerically, and these are in Table 1. Therefore the reduced system (4.12) can be rewritten as the following:

$$\begin{cases} \dot{u}_0 = \tilde{\sigma} u_0 - \sum h^0_{i_0 i_1 i_2}\, u_0^{i_0} u_1^{i_1} u_2^{i_2} + \text{ h.o.t.}, \\ \dot{u}_1 = \tilde{\sigma} u_1 - \omega u_2 - \sum h^1_{i_0 i_1 i_2}\, u_0^{i_0} u_1^{i_1} u_2^{i_2} + \text{ h.o.t.}, \\ \dot{u}_2 = \tilde{\sigma} u_2 + \omega u_1 - \sum h^2_{i_0 i_1 i_2}\, u_0^{i_0} u_1^{i_1} u_2^{i_2} + \text{ h.o.t.}, \end{cases} \tag{4.14}$$

where the summations are over nonnegative integers i_0, i_1, i_2 such that $i_0 + i_1 + i_2 = 3$ and *h.o.t.* means *higher order terms*. We rewrite (4.14) in the compact form

$$\dot{u} = \tilde{\sigma} u + \omega \cdot T u + H(u) + \text{h.o.t.}, \tag{4.15}$$

where

$$T u = \begin{pmatrix} 0 & 0 & 0 \\ 0 & 0 & -1 \\ 0 & 1 & 0 \end{pmatrix} \cdot \begin{pmatrix} u_0 \\ u_1 \\ u_2 \end{pmatrix} \tag{4.16}$$

and $H(u)$ is the vector-valued homogeneous cubic polynomials of u_0, u_1, u_2 in (4.14), including the minus sign.

5 Derivation of the Normal Form

5.1 Elimination of the nonresonant terms

To investigate the dynamics of the reduced system (4.14), following [10] we perform a polynomial transformation of coordinates to obtain its normal form. Let $\mathbb{H}_3$ be the space of homogeneous polynomials of degree 3. We can regard $H(u)$ in equation (4.15) as an element in the space $\mathbb{H}_3 \oplus \mathbb{H}_3 \oplus \mathbb{H}_3 = \overrightarrow{\mathbb{H}_3}$, a basis of which is given by

$$\left\{u_1^3,\, u_1^2u_2,\, u_1^2u_0,\, u_1u_2^2,\, u_1u_2u_0,\, u_1u_0^2,\, u_0^3,\, u_1^2u_0,\, u_1u_0^2,\, u_0^3\right\} \otimes \left\{ \begin{pmatrix} 1 \\ 0 \\ 0 \end{pmatrix}, \begin{pmatrix} 0 \\ 1 \\ 0 \end{pmatrix}, \begin{pmatrix} 0 \\ 0 \\ 1 \end{pmatrix} \right\}. \tag{5.1}$$

Consider a transformation of the form

$$(u_0, u_1, u_2) = (v_0, v_1, v_2) + P(v_0, v_1, v_2), \tag{5.2}$$

where $P \in \overrightarrow{\mathbb{H}_3}$ is a vector-valued homogeneous cubic polynomial. We substitute (5.2) into (4.15) to find

$$\dot{v} = \tilde{\sigma} v + \omega \cdot Tv + H(v) + \mathrm{ad}T(P)(v) + \text{h.o.t.}. \tag{5.3}$$

Here the adjoint operator $\mathrm{ad}T(\cdot) : \overrightarrow{\mathbb{H}_3} \to \overrightarrow{\mathbb{H}_3}$ in above equation is defined by

$$\mathrm{ad}\, T(P)(v) = TP(v) - (DP) \cdot Tv, \quad \forall P \in \overrightarrow{\mathbb{H}_3}, \tag{5.4}$$

where $DP = (\partial_j P_i)$ is the 3×3 matrix. We shall write $H(v) = H_1(v) + H_2(v)$, where $H_1 \in \mathrm{Ker}(\mathrm{ad}\, T)$ and $H_2 \in \mathrm{Range}(\mathrm{ad}\, T)$. Then by an appropriate choice of P such that $\mathrm{ad}\, T(P) = -H_2$, the cubic terms $H(v) + \mathrm{ad}\, T(P)(v)$ will reduce to $H_1(v)$, i.e. the projection of the $H(v)$ onto the kernel $\mathrm{Ker}(\mathrm{ad}\, T)$.

To carry out this reduction, we let $\mathrm{ad}\, T(\cdot)$ defined in (5.4) act on each vector of the basis (5.1) and expand the result in the same basis to find $\mathrm{ad}\, T(\cdot)$ has the following matrix

$$\mathrm{ad}\, T = \begin{pmatrix} \mathbb{S}_{10} & \mathbb{O} & \mathbb{O} \\ \mathbb{O} & \mathbb{S}_{10} & -\mathbb{I}_{10} \\ \mathbb{O} & \mathbb{I}_{10} & \mathbb{S}_{10} \end{pmatrix}, \tag{5.5}$$

where $\mathbb{I}_{10}$ is 10 dimensional identity matrix, $\mathbb{O}$ is the 10×10 zero matrix and

$$\mathbb{S}_{10} = \begin{pmatrix} 0 & -1 & 0 & 0 & 0 & 0 & 0 & 0 & 0 & 0 \\ 3 & 0 & 0 & -2 & 0 & 0 & 0 & 0 & 0 & 0 \\ 0 & 0 & 0 & 0 & -1 & 0 & 0 & 0 & 0 & 0 \\ 0 & 2 & 0 & 0 & 0 & 0 & -3 & 0 & 0 & 0 \\ 0 & 0 & 2 & 0 & 0 & 0 & 0 & -2 & 0 & 0 \\ 0 & 0 & 0 & 0 & 0 & 0 & 0 & 0 & -1 & 0 \\ 0 & 0 & 0 & 1 & 0 & 0 & 0 & 0 & 0 & 0 \\ 0 & 0 & 0 & 0 & 1 & 0 & 0 & 0 & 0 & 0 \\ 0 & 0 & 0 & 0 & 0 & 1 & 0 & 0 & 0 & 0 \\ 0 & 0 & 0 & 0 & 0 & 0 & 0 & 0 & 0 & 0 \end{pmatrix}. \tag{5.6}$$

a_1	a_2	b_1	b_2	c_1	c_2
0.083	−0.096	−0.130	−0.422	0.003	−0.090

Table 2: The value of the coefficients in the computed normal form (5.9).

Using Maple to investigate matrix (5.5), we find that $\operatorname{ad} T$ is diagonalizable (in the complex sense) and its nullspace is a six dimensional subspace of $\overrightarrow{\mathbb{H}_3}$ spanned by the following eigenvectors:

$$\begin{pmatrix} r^2 v_0 \\ 0 \\ 0 \end{pmatrix}, \begin{pmatrix} v_0^3 \\ 0 \\ 0 \end{pmatrix}, \begin{pmatrix} 0 \\ r^2 v_1 \\ r^2 v_2 \end{pmatrix}, \begin{pmatrix} 0 \\ v_1 v_0^2 \\ v_2 v_0^2 \end{pmatrix}, \begin{pmatrix} 0 \\ -r^2 v_2 \\ r^2 v_1 \end{pmatrix}, \begin{pmatrix} 0 \\ -v_2 v_0^2 \\ v_1 v_0^2 \end{pmatrix}, \tag{5.7}$$

where for convenience we defined $r = r(v) = \sqrt{v_1^2 + v_2^2}$. On the other hand, the remaining twenty-four eigenvectors of $\operatorname{ad} T$ corresponding to nonzero eigenvalues span the range of $\operatorname{ad} T$ and can therefore be transformed away by an appropriate choice of P in (5.2). Thus the system (4.12) can be transformed to the following simplified form :

$$\begin{cases} \dot{v_0} = \tilde{\sigma} v_0 + a_1 r^2 v_0 + a_2 v_0^3 + \text{h.o.t.}, \\ \dot{v_1} = \tilde{\sigma} v_1 + \omega v_1 + b_1 r^2 v_1 + b_2 v_1 v_0^2 - c_1 r^2 v_2 - c_2 v_2 v_0^2 + \text{h.o.t.}, \\ \dot{v_2} = \tilde{\sigma} v_2 - \omega v_2 + b_1 r^2 v_2 + b_2 v_2 v_0^2 + c_1 r^2 v_2 + c_2 v_1 v_0^2 + \text{h.o.t.}. \end{cases} \tag{5.8}$$

Using Maple to perform the computations, we find that the coefficients in Table 1 lead to a reduced system (5.8) with the coefficients $a_{1,2}$, $b_{1,2}$ and $c_{1,2}$ given in Table 2.

5.2 Scaling of the remaining terms

We introduce polar coordinates such that $v_1 = r\cos\theta$ and $v_2 = r\sin\theta$ and for convenience we define $z = v_0$. Then the system (5.8) can be rewritten as the following

$$\begin{cases} \dot{z} = z(\tilde{\sigma} + a_1 r^2 + a_2 z^2) + \mathcal{O}(|r,z|^4), \\ \dot{r} = r(\tilde{\sigma} + b_1 r^2 + b_2 z^2) + \mathcal{O}(|r,z|^4), \\ \dot{\theta} = \omega + \mathcal{O}(|r,z|^2). \end{cases} \tag{5.9}$$

We study the reduced bifurcation problem in the variables r and z. By scaling these variables

$$\tilde{z} = z \cdot \sqrt{-a_2}, \quad \tilde{r} = r \cdot \sqrt{-b_1}, \tag{5.10}$$

we may reduce this subsystem of (5.9) to the *normal form*

$$\begin{cases} \frac{d}{dt}\tilde{z} = \tilde{z}(\tilde{\sigma} - m\tilde{r}^2 - \tilde{z}^2) + \mathcal{O}(|\tilde{r},\tilde{z}|^4), \\ \frac{d}{dt}\tilde{r} = \tilde{r}(\tilde{\sigma} - n\tilde{z}^2 - \tilde{r}^2) + \mathcal{O}(|\tilde{r},\tilde{z}|^4), \end{cases} \tag{5.11}$$

where

$$m = \frac{a_1}{b_1} \approx -0.64, \quad \text{and} \quad n = \frac{b_2}{a_2} \approx 4.40. \tag{5.12}$$

Since to lowest order $\dot{\theta}$ is a constant, an equilibrium of (5.11) with $r \neq 0$ corresponds to a periodic solution of (5.9).

6 Analysis of the Bifurcation

In previous sections for the case $\Lambda^{-1} = \Lambda_c^{-1}$ exactly, we derived equation (5.9) for the restriction of (4.1) to the center manifold. Let us show that Equation (5.9) undergoes both a Hopf bifurcation and steady state bifurcation as $\tilde{\sigma}$ passes through zero. Motivated by [11, 12], we expect that interactions between the two modes can lead to secondary bifurcations.

Neglecting the h.o.t. in (5.11) and dropping the tildes on $\tilde{r}$, $\tilde{z}$, we obtain the system

$$\begin{pmatrix} \dot{z} \\ \dot{r} \end{pmatrix} = f(z, r, \tilde{\sigma}) = \begin{pmatrix} z(\tilde{\sigma} - mr^2 - z^2) \\ r(\tilde{\sigma} - nz^2 - r^2) \end{pmatrix}. \tag{6.1}$$

Note that this system has $\mathbb{Z}_2 \oplus \mathbb{Z}_2$ symmetry under the transformations $z \to -z$ and $r \to -r$. This symmetry helps in the enumeration of equilibria $f(r, z, \tilde{\sigma}) = 0$ of (6.1). Specifically, we have the four possible cases

- the trivial zero solution $(0, 0)$;
- a pure z–mode $(\pm\sqrt{\tilde{\sigma}}, 0)$, corresponding to a standing wave solution;
- a pure r–mode $(0, \sqrt{\tilde{\sigma}})$, corresponding to a periodic solution of (5.9);
- mixed mode which satisfies

$$\tilde{\sigma} = mr^2 + z^2 = nz^2 + r^2. \tag{6.2}$$

The pure z–mode and the pure r–mode appear only while $\tilde{\sigma} \geq 0$, i.e., both modes bifurcate supercritically. Regarding possible mixed modes, given m and n as in (5.12) there is no value of $\tilde{\sigma}$ for which (6.2), a pair of linear equation in r^2 and z^2, has real nonzero solutions. Checking the eigenvalues of $df(z, r, \tilde{\sigma})$, we find when $\tilde{\sigma} < 0$, the trivial zero solution is stable; and when $\tilde{\sigma} > 0$, only the pure z–mode is stable. We summarize this information in the schematic bifurcation diagram Figure 5, where a solid line means stable and dashed line means unstable.

More generally, we assume Λ^{-1} in (1.3) is close to, but not exactly equal to, Λ_c^{-1}. As illustrated in Figure 1, changing Λ^{-1} shifts both Ω_0 and $\operatorname{Re}\Omega_{1,2}$. To model these shifts we consider an unfolding[13, 14] of (6.1) with two auxiliary parameters μ_1 and μ_2:

$$\begin{pmatrix} \dot{z} \\ \dot{r} \end{pmatrix} = \begin{pmatrix} z(\tilde{\sigma} - \mu_1 - mr^2 - z^2) \\ r(\tilde{\sigma} - \mu_2 - nz^2 - r^2) \end{pmatrix}. \tag{6.3}$$

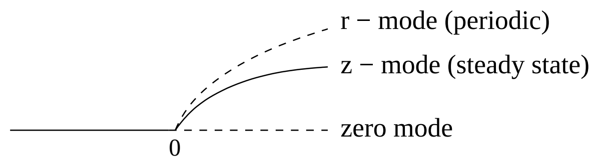

Figure 5: Schematic bifurcation diagram to the system (5.11), where the horizontal direction denotes the value of $\tilde{\sigma}$. The z–mode represents a symmetric pair of steady solutions of (5.9), and the r–mode represents a periodic solution of (5.9). A solid line means the mode is stable, and a dashed line means it is unstable.

Letting $\bar{\sigma} = \tilde{\sigma} - \mu_2$ and $\mu = \mu_1 - \mu_2$, we may eliminate an inessential parameter and rewrite (6.3) in the following form:

$$\begin{pmatrix} \dot{z} \\ \dot{r} \end{pmatrix} = F(z, r, \bar{\sigma}, \mu) = \begin{pmatrix} (\bar{\sigma} - \mu)z - mr^2 z - z^3 \\ \bar{\sigma} r - nrz^2 - r^3 \end{pmatrix}. \tag{6.4}$$

As above, we can enumerate equilibria of (6.4) — solutions of $F(z, r, \bar{\sigma}, \mu) = 0$ — in four cases.

- the trivial zero solution $(0, 0)$;
- for $\bar{\sigma} > \mu$, a pure z–mode $(\pm\sqrt{\bar{\sigma} - \mu}, 0)$, corresponding to a standing wave solution;
- for $\bar{\sigma} > 0$, a pure r–mode $(0, \sqrt{\bar{\sigma}})$, corresponding to a periodic solution;
- a mixed mode which satisfies $\bar{\sigma} = mr^2 + z^2 + \mu = nz^2 + r^2$.

The stability of the bifurcating solutions and the existence of (real) mixed-mode solutions depend on the sign of μ.

Case I : $\mu < 0$. In this case there are no mixed-mode solutions for any value of $\bar{\sigma}$. Thus the equilibria of (6.4) trace out a bifurcation diagram as sketched in Figure 6A. Exchange of stability suggests that the trivial solution for $\bar{\sigma} < \mu$ and the z–mode for $\bar{\sigma} > \mu$ are stable and other solutions are unstable. This is easily confirmed from the Jacobian of (6.4).

Case II : $\mu > 0$. In this case, the mixed-mode equations may be solved to obtain

$$r^2 = \frac{(n-1)\bar{\sigma} - n\mu}{mn - 1}, \quad z^2 = \frac{(m-1)\bar{\sigma} + \mu}{mn - 1}. \tag{6.5}$$

In the range $\delta_1 < \bar{\sigma} < \delta_2$, where

$$\delta_1 = \frac{\mu}{1 - m} \quad \text{and} \quad \delta_2 = \frac{n\mu}{n - 1}, \tag{6.6}$$

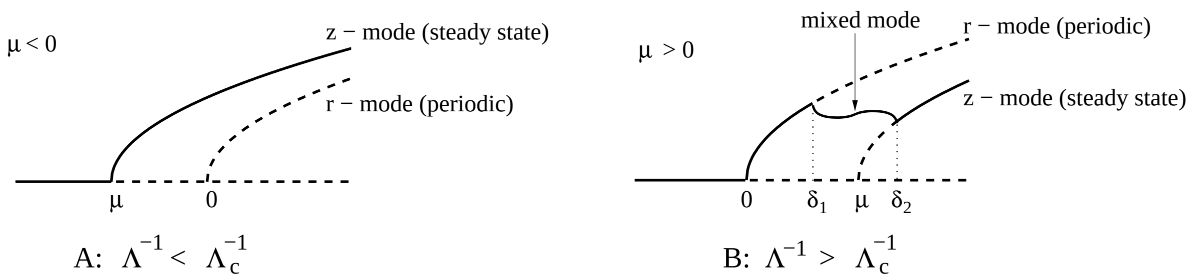

Figure 6: Schematic bifurcation diagrams for two cases $\Lambda^{-1} < \Lambda_c^{-1}$ and $\Lambda^{-1} > \Lambda_c^{-1}$, where the horizontal direction denotes the value of $\bar{\sigma}$. The solid line means the mode is stable and the dashed line means it is unstable.

both right-hand-sides of (6.5) are positive. Thus (real) mixed-mode solutions exist for this range of $\bar{\sigma}$. Since $z \to 0$ as $\bar{\sigma} \to \delta_1^+$ and $r \to 0$ as $\bar{\sigma} \to \delta_2^-$, the mixed-mode solution branch connects the pure r– and z–modes, as sketched in Figure 6B. Exchange of stability suggests the stability assignments of the figure, and these are readily verified. Speaking teleologically, we may say that the secondary bifurcations of the mixed-mode solution are needed for the primary branches to have the same stability as in Figure 5 for large $\bar{\sigma}$.

These bifurcation diagrams agree with the simulations. For fixed $\Lambda^{-1} < \Lambda_c^{-1}$, when we increase σ from 0, the simulations in Figure 2 show a steady state bifurcation from the trivial solution to a standing wave solution, which is the behavior in the bifurcation diagram Figure 6A. For fixed $\Lambda^{-1} > \Lambda_c^{-1}$, when we increase σ from 0, Figure 2 shows we first encounter a bifurcation from the trivial solution to a pure r–mode (periodic solution with zero average, to leading order), and then it bifurcates to a mixed mode (periodic solution with nonzero average), finally it bifurcates to the pure z–mode (standing wave solution), all of which can be observed from Figure 6B as we increases $\bar{\sigma}$.

The above data also provide a check on the accuracy of truncating all h.o.t.. We can obtain δ_1 and δ_2 from the simulation in Figure 3, where $\Lambda^{-1} = 3.3$. δ_1 represents the increase in $\bar{\sigma}$, or equivalently of σ, from the first bifurcation (emergence of the pure r–mode) to the second bifurcation (the appearance of the mixed mode), and similarly δ_2 represents the increase in $\bar{\sigma}$ or σ from the first bifurcation to the third. We find

$$\delta_1\big|_{\text{sim}} \approx 3.32 - 3.14 = 0.18, \quad \delta_2\big|_{\text{sim}} \approx 3.49 - 3.14 = 0.35.$$

On the other hand, since $\mu = \mu_1 - \mu_2$, where to the leading order μ_1 and μ_2 are shifts of the threshold values of $\tilde{\sigma}$ for the emergence of pure z–mode and r–mode respectively, we obtain $\mu = \operatorname{Re}\Omega_1 - \Omega_0$. By computation of the eigenvalues, as shown in Fig 1, when $\Lambda^{-1} = 3.3$, we have $\mu \approx 0.28$. Thus the formula in (6.6) gives the theoretical result:

$$\delta_1\big|_{\text{th}} = \frac{\mu}{1-m} \approx 0.17, \quad \delta_2\big|_{\text{th}} = \frac{n\mu}{n-1} \approx 0.36$$

for the values of m and n in (5.12), which matches the simulated result well.

7 Conclusion

We have studied the bifurcations of the modulation equation (1.3) for APD alternans propagating on a cardiac fiber. We observed the solutions undergo either a steady state or a Hopf bifurcation; which occurs first depends on one parameter in the equation, the nondimensional Λ^{-1} defined in (2.1). There is one special value Λ_c^{-1} so that we have a codimension 2 bifurcation for $\Lambda^{-1} = \Lambda_c^{-1}$; if Λ^{-1} is near Λ_c^{-1}, there is competition between multiple modes, which leads to the following: 1) for $\Lambda^{-1} < \Lambda_c^{-1}$, the equation (1.3) has a simple steady state bifurcation as we increase the bifurcation parameter σ; 2) for $\Lambda^{-1} > \Lambda_c^{-1}$ we will encounter a Hopf bifurcation followed by secondary bifurcations and finally we will reach a standing wave solution for σ sufficiently large.

We also observe an interesting phenomenon: the amplitude of alternans at the stimulus site is quite different for the steady state and the periodic solution. For instance, the pure z–mode (standing wave solution, as shown in Fig 2B, upper graph) has an nonzero constant value at the stimulus site, but the pure r–mode solution (pure periodic, as shown in Fig 2 B, bottom) almost has no amplitude of oscillation at $x = 0$. This can be seen from the eigenfunctions $\phi_j' s$ (see Figure 4A). The z–mode is approximately given by ϕ_0 and the r–mode, by $\phi_{1,2}$. The different behavior between ϕ_0 and $\phi_{1,2}$ induces the great change of the amplitude of solution at $x = 0$.

Throughout this paper, the dimensionless cardiac fiber length is assumed to be $l = 6$. However, the dynamical behavior of (1.3) is similar for any l greater than 6. In perticular, the evolution of eigenvalues has the same behavior as in Figure 1 when we increase Λ^{-1}. For smaller l the behavior of (1.3) is different, as we shall explore in a future paper.

We also mention here that for Λ^{-1} in a broader neighbourhood of Λ_c^{-1}, possibly far away from Λ_c^{-1}, (1.3) may have more complicated dynamic, including chaos, which we shall show in a future paper.

Acknowledgments

We gratefully acknowledge the support of the National Institutes of Health under grant 1R01-HL-72831 and the National Science Foundation under grant PHY-0549259.

References

[1] R. F. Gilmour Jr. and D. R. Chialvo, *Electrical restitution, Critical mass, and the riddle of fibrillation*, J. Cardiovasc. Electrophysiol. 10(1999), 1087-1089.

[2] A. Garfinkel *et al.*, *Preventing Ventricular Fibrillation by Flattening Cardiac Restitution*, Proc. Natl. Acad. Sci. USA 97 (2000), 6061-6066.

[3] A. V. Panfilov, *Spiral breakup as a model of ventricular fibrillation*, Chaos 8 (1998), 57-64.

[4] J. B. Nolasco and R.W. Dahlen, *A graphic method for the study of alternation in cardiac action potentials*, J Appl Physiol 25 (1968), 191-196.

[5] M. R. Guevara *et al.*, *Electrical alternans and period doubling bifurcations*, Proceedings of the 11th Computers in Cardiology Conference, IEEE Computer Society, Los Angeles (1984), 167-170.

[6] B. Echebarria and A. Karma, *Instability and spatiotemporal dynamics of alternans in paced cardiac tissue*, Phys. Rev. Lett. 88(2002), 208101.

[7] B. Echebarria and A. Karma, *Amplitude-equation approach to spatiotemporal dynamics of cardiac alternans*, Phys. Rev. E 76(2007), 051911.

[8] S. Dai and D.G. Schaeffer, *Spectrum of a linearized amplitude equation for alternans in a cardiac fiber*, SIAM J. Appl. Math., accepted.

[9] J. Carr, *Applications of Centre Manifold Theory*, Springer-Verlag, New York, 1981.

[10] J. Guckenheimer and P. Holmes, *Nonlinear Oscillations, Dyanamical Systems, and Bifurcations of Vector Fields*, Springer-Verlag, New York, 1983.

[11] W. F. Langford, *Periodic and steady state interactions lead to tori*, SIAM J. Appl. Math. 37(1979), 22-48.

[12] J. Guckenheimer, *On a Codimension Two bifurcation*, Lecture Notes in Mathematics 898(1981), 99-142.

[13] P. Holmes, *Unfolding a degenerate nonlinear oscillator: a codimension two bifurcation*, In *Nonlinear Dynamics*, R. H. G. Helleman (ed.), (1980) 473-488. New York Academy of Sciences: New York.

[14] M. Golubitsky and D.G. Schaeffer, *Singularities and Groups in Bifurcation Theory*, Springer-Verlag, New York, 1985.